Surface Science 202 (1988) 1–31
North-Holland, Amsterdam

AN ANALYSIS OF THE EFFECT OF DEFECT STRUCTURES ON CATALYTIC SURFACES BY THE BOUNDARY ELEMENT TECHNIQUE

Anthony P. PEIRCE

Program in Applied and Computational Mathematics, Princeton University, Princeton, NJ 08544, USA

and

Herschel RABITZ

Department of Chemistry, Princeton University, Princeton, NJ 08544, USA

Received 15 December 1987; accepted for publication 31 March 1988

The boundary element (BE) technique is used to analyze the effect of defects on one-dimensional chemically active surfaces. The standard BE algorithm for diffusion is modified to include the effects of bulk desorption by making use of an asymptotic expansion technique to evaluate influences near boundaries and defect sites. An explicit time evolution scheme is proposed to treat the non-linear equations associated with defect sites. The proposed BE algorithm is shown to provide an efficient and convergent algorithm for modelling localized non-linear behavior. Since it exploits the actual Green's function of the linear diffusion–desorption process that takes place on the surface, the BE algorithm is extremely stable.

The BE algorithm is applied to a number of interesting physical problems in which non-linear reactions occur at localized defects. The Lotka–Volterra system is considered in which the source, sink and predator–prey interaction terms are distributed at different defect sites in the domain and in which the defects are coupled by diffusion. This example provides a stringent test of the stability of the numerical algorithm. Marginal stability oscillations are analyzed for the Prigogine–Lefever reaction that occurs on a lattice of defects. Dissipative effects are observed for large perturbations to the marginal stability state, and rapid spatial reorganization of uniformly distributed initial perturbations is seen to take place. In another series of examples the effect of defect locations on the balance between desorptive processes on chemically active surfaces is considered. The effect of dynamic pulsing at various time-scales is considered for a one species reactive trapping model. Similar competitive behavior between neighboring defects previously observed for static adsorption levels is shown to persist for dynamic loading of the surface. The analysis of a more complex three species reaction process also provides evidence of competitive behavior between neighboring defect sites. The proposed BE algorithm is shown to provide a useful technique for analyzing the effect of defect sites on chemically active surfaces.

1. Introduction

The need to understand the influence of surface defect structures on catalytic phenomena is a topic of considerable importance. Practical catalytic

0039-6028/88/$03.50

reactors are likely to contain active surfaces with high coverages of defect structures due to faulting or foreign substances.

A number of different theoretical analyses of the effect of defect structures in an environment of diffusion, adsorption, and desorption have been considered. Serri et al. [1] have used a discrete step approach to analyze the effect of defect structures on desorption kinetics. A more macroscopic analysis of the effect of defect structures assumes that the number of inter-defect sites is sufficiently large for a continuum approximation to be valid. The current authors [2] have demonstrated that the continuum assumption is remarkably good even when the number of inter-defect sites is as low as 20. Analyses based on the continuum assumption include a linear boundary-condition-reaction model that was used to consider the effect of a single defect [3], an effective medium approach that was used to consider the reaction between a single species and a set of randomly distributed reaction sites [4], far from equilibrium phenomena that have been investigated for a single active site in an infinite medium [5], and cooperative instability phenomena that have been investigated for arrays of catalytic sites [6].

Numerical studies of continuum models of defect structures include the use of the multigrid finite difference method with elongated Gaussian representations of defect structures to determine the steady states of a system involving diffusion, adsorption, and many species [7]; as well as the use of an alternating direction implicit (ADI) finite element method for the time dependent analysis of defect structures represented by elongated Gaussians [8]. In both of these analyses the representation of defects at arbitrary locations in the domain without significant mesh deformations is difficult. The method outlined in the present paper may be applied to the latter problem, and such an application will be considered in a following paper [13].

In this paper we consider the use of the boundary element (BE) method to represent the effect of defect structures at arbitrary locations on catalytic surfaces. We assume that the bulk diffusion, adsorption, and desorption processes are linear while non-linear reactions occur at arbitrarily located defects. The BE technique enables one to invert analytically the linear differential operator that describes bulk diffusion and desorption processes. The resulting integral equation, which involves the Green's function for the diffusing–desorbing bulk, provides an elegant representation of the localized non-linear reaction.

The numerical algorithm described here differs from the standard BE technique [9–11] in two essential features. Firstly, the effect of bulk desorption has to be incorporated into the Green's function. This necessitates the use of an asymptotic expansion technique to calculate accurately the solution near boundaries and active sites. Secondly, the non-linear localized reactions at defects result in an additional integral being added to the standard boundary integral equation for heat conduction [9]. This separation of linear and

non-linear effects enables the effects of localized sites at arbitrary locations to be incorporated without having to disturb the mesh used to evolve the linear part of the solution. This overlay feature is particularly useful if the effects of randomly distributed defects are to be included [7]. In addition, the BE technique is shown to provide an extremely stable algorithm as it exploits the actual Green's function of the stable linear diffusion–desorption process taking place in the bulk medium. The integral representation of the localized non-linear effects also allows the solution to be evolved explicitly without requiring the solution of a system of non-linear equations at each time-step. In another work [12] the convergence properties of the BE technique are investigated with and without localized non-linear reactions. The results of this analysis are summarized here. This paper focuses exclusively on one-dimensional problems. The extension to two-dimensional surfaces is considered in another paper [13].

This paper is organized as follows: Section 2 introduces the governing equations of the continuum defect model. In section 3 we discuss the boundary integral formulation of the problem, the discretization of the boundary integral equations, the explicit treatment of non-linear localized reaction terms, and the convergence properties of the algorithm. In section 4 we apply the BE technique to four physical problems that demonstrate both the stability of the numerical technique and a number of interesting cooperative/competitive phenomena associated with defect structures. In section 5 we summarize the results and make some concluding remarks.

2. Governing equations

2.1. Initial-boundary value problem for linear diffusion and localized non-linear reaction

The equations governing the diffusion, adsorption–desorption and localized reaction are taken to be [5,6]

$$\frac{\partial \boldsymbol{u}}{\partial t} = D\frac{\partial^2 \boldsymbol{u}}{\partial x^2} - \Omega \boldsymbol{u} + \sum_{l=1}^{L} \boldsymbol{R}_l(\boldsymbol{u})\delta(x - x_l) + \boldsymbol{f}, \quad x, x_l \in (x_0, x_N). \tag{2.1}$$

Here $\boldsymbol{u}(x, t) \in \mathbb{R}^{+S}$ is a vector with positive valued components representing the concentrations of the S different species, D is a matrix of diffusion coefficients, Ω is a matrix representing desorption or linear bulk reaction, $\boldsymbol{R}_l$ are the rate terms due to reactions taking place at the active site x_l, and $\boldsymbol{f}(x, t)$ is the incident flux due to adsorption. We assume that the bulk is homogeneous so that D and Ω are constant and that the bulk processes are decoupled so that D and Ω are diagonal. In addition, coverage is taken as sufficiently low that $\boldsymbol{f}$ is not dependent on the local concentrations.

In order to be able to determine the solution $\boldsymbol{u}$ of (2.1) we prescribe an initial condition

$$\boldsymbol{u}(x, 0) = \boldsymbol{u}^0(x) \tag{2.2a}$$

and appropriate boundary conditions of the general form:

$$\left(\alpha_i \frac{\partial}{\partial x} + \beta_i\right)\boldsymbol{u}(x_i, t) = \boldsymbol{g}_i(t), \; i = 0, \; N. \tag{2.2b}$$

Here $\boldsymbol{g}_i$ is a specified function. As was the case with the bulk, we assume that the boundary conditions are decoupled so that α_i and β_i are diagonal. Hence the only coupling in the equations governing the various species occurs through the, in general, non-linear reaction term $\boldsymbol{R}_l$.

Physically these equations represent localized reactions that occur on a number of parallel chemically active "lines" or steps on a two-dimensional surface in which linear diffusion and adsorption–desorption are taking place. Eqs. (2.1) and (2.2) also provide a one-dimensional model for a more general problem comprising a surface on which adsorption–desorption and linear diffusion are taking place, while generally non-linear reaction processes may occur at localized defects in the form of curves on the surface.

2.2. Alternative "jump-condition" form

It is possible to rewrite (2.1) in an alternative form if we assume that $\boldsymbol{u}, \boldsymbol{f} \in C^0(x_0, x_N)$. We integrate (2.1) over each of the intervals $(x_l - \epsilon, \; x_l + \epsilon)$, $l = 1, \ldots, L$ in turn letting $\epsilon \to 0^+$ in each case. An application of the mean value theorem for integrals yields the following conditions:

$$\boldsymbol{D}\left[\frac{\partial \boldsymbol{u}}{\partial x}\right]_{x_l} = -\boldsymbol{R}_l(u)|_{x_l}, \quad l = 1, \ldots, L. \tag{2.3}$$

Here

$$\left[\frac{\partial \boldsymbol{u}}{\partial x}\right]_{x_l} := \lim_{\epsilon \to 0^+}\left(\frac{\partial \boldsymbol{u}}{\partial x}(x_l + \epsilon, t) - \frac{\partial \boldsymbol{u}}{\partial x}(x_l - \epsilon, t)\right).$$

The initial-boundary value problem (2.1)–(2.2) can now be replaced by the linear PDE obtained by setting $\boldsymbol{R}_l \equiv \boldsymbol{0}$ in (2.1) and requiring that solutions satisfy not only (2.2) but also the additional jump conditions (2.3). This alternative form emphasizes the fact that we have a linear differential equation the solution of which is subject to non-linear ancillary conditions. These ancillary conditions reduce to boundary conditions in some special cases. For example, we could assume that the solution $\boldsymbol{u}$ is constant throughout (x_0, x_N) except for a single subinterval $[x_l, x_{l+1}]$. In this case the jump conditions which apply at x_l and x_{l+1} reduce to derivative boundary conditions.

3. The boundary element algorithm

3.1. The boundary integral formulation of the diffusion-localized reaction equation

The starting point of this formulation is the use of the method of Green's functions to rewrite (2.1) as an integral equation involving boundary values of the solution and its derivatives, initial values, and sources that are distributed throughout the interval (x_0, x_N). As this technique is standard, the derivation will be omitted [9–11]. Let

$$\gamma(x) = \begin{cases} 0, & x \notin [x_0, x_N], \\ 1, & x \in (x_0, x_N), \end{cases}$$

then

$$\begin{aligned} \gamma(x)u(x, t) &= \int_{x_0}^{x_N} G(x-\xi, t)u^0(\xi)\,\mathrm{d}\xi \\ &\quad + \int_0^t \left[G(x-\xi, t-\tau)D\frac{\partial u}{\partial \xi}(\xi, \tau) - \frac{\partial G}{\partial \xi}(x-\xi, t-\tau)Du(\xi, \tau) \right]_{\xi=x_0}^{\xi=x_N} \mathrm{d}\tau \\ &\quad + \int_0^t \int_{x_0}^{x_N} G(x-\xi, t-\tau)F(\xi, \tau)\,\mathrm{d}\xi\,\mathrm{d}\tau. \end{aligned} \tag{3.1}$$

Here

$$L_\xi G(\xi - x, \tau - t) := \left(D\frac{\partial^2}{\partial \xi^2} - \Omega - I\frac{\partial}{\partial \tau} \right) G(\xi - x, \tau - t) := -\delta(\xi - x)\delta(\tau - t)I$$

and in addition $G \to 0$ as $|x| \to \infty$ and G satisfies the causality condition $G(x, t) = 0$ if $t < 0$.

The explicit expression for G can be derived using Fourier or Laplace transforms [14,15]:

$$\begin{aligned} G_{ij}(x, t) &= H(t)\frac{\exp\left(-\Omega_i t - x^2/4D_i t\right)}{2\sqrt{\pi D_i t}}\delta_{ij}, \quad i, j = 1, \ldots, s, \\ H(t) &= \begin{cases} 1, & t \geq 0, \\ 0, & t < 0. \end{cases} \end{aligned} \tag{3.2}$$

This Green's function differs from that for the standard diffusion equation through the term $\exp(-\Omega_i t)$, which is due to desorption. Notice that in (3.1)

the localized reaction terms have been lumped with the source term f by defining

$$F = \sum_{l=1}^{L} R_l(u)\delta(x - x_l) + f.$$

If we substitute this expression for F into (4.1) we obtain

$$\gamma(x)u = \int_{x_0}^{x_N} Gu^0 \, d\xi + \int_0^t \int_{x_0}^{x_N} Gf \, d\xi \, d\tau + \int_0^t \left\{ \left[GD\frac{\partial u}{\partial \xi} - \frac{\partial G}{\partial \xi} Du \right]_{\xi=x_0}^{\xi=x_N} + \sum_{l=1}^{L} G(x - x_l, t - \tau) R_l(u(x_l, \tau)) \right\} d\tau. \tag{3.3}$$

Here the arguments of some of the terms have been omitted for the sake of brevity.

Consider the implications of (3.1) for a well-posed boundary value problem such as (2.1)–(2.2) in the absence of localized reactions i.e. $F = f$. In this case (3.1) is an expression of the solution in terms of quadratures of the prescribed functions u^0 and f and an integral involving the values of u and its derivative $\partial u/\partial \xi$ at the boundary points x_0 and x_N. If we were for example considering Neumann boundary conditions ($\alpha_i = l$, $\beta_i = 0$ in (2.2b)), then all that prevents us from writing down the solution $u(x, t)$ is the unknown values of u at x_0 and x_N. If we let $x \to x_0$ and x_N in turn, we obtain two integral equations from which $u(x_i, t)$, $i = 0, N$ can in principle be found. Once $u(x_i, t)$, $i = 0, N$ are known, the solution at any point (x, t) can be found by direct quadrature using (3.1). The full variety of boundary value problems as represented by (2.2b) can be solved in an analogous way. Due to the singularity of the kernel $\partial G/\partial \xi$ in (3.1), special care has to be exercised in the limiting process $x \to x_i$, $i = 0, N$ used to derive the boundary integral equations. The resulting integral equations are

$$\begin{aligned} &\tfrac{1}{2}u(x_i, t) \\ &= \int_{x_0}^{x_N} G(x_i - \xi, t)u^0(\xi) \, d\xi \\ &\quad + \int_0^{t-0} \left[G(x_i - \xi, t - \tau) D\frac{\partial u}{\partial \xi}(\xi, \tau) - \frac{\partial G}{\partial \xi}(x_i - \xi, t - \tau) Du(\xi, \tau) \right]_{\xi=x_0}^{\xi=x_N} d\tau \\ &\quad + \int_0^{t-0} \int_{x_0}^{x_N} G(x_i - \xi, t - \tau) F(\xi, \tau) \, d\xi \, d\tau, \quad i = 0, N. \end{aligned} \tag{3.4}$$

Here $\int_0^{t-0}$ is used to indicate that a small neighborhood $(t - \epsilon, t)$ is to be excluded in the evaluation of that integral. Notice, by defining $\gamma(x_i) = \frac{1}{2}$, $i = 0, N$ eq. (3.3) can be made to encompass (3.4) as a special case.

If localized reactions are present, then the appropriate integral equations can, as in the case of (3.2), be obtained by substituting

$$F = f + \sum_{l=1}^{L} R_l \delta(x - x_l)$$

into (3.3). In this case the resulting integral equations not only involve unknowns on the boundary, but also unknowns at the localized active sites that appear in a non-linear form.

3.2. Space–time discretization

The space–time region $[x_0, x_N] \times [0, T]$ is divided into cells $[x_e, x_{e+1}] \times [t_j, t_{j+1}]$, $e = 0, \ldots, N-1$; $j = 0, \ldots, M-1$. Over this mesh of space–time cells we construct piecewise polynomial basis functions in terms of which the solution u, the derivative $\partial u/\partial \xi$, and the specified functions f, g and u^0 are expanded. These expansions are substituted into (3.3), and the products of the Green's function and the piecewise polynomial basis functions are integrated to form the appropriate influence matrices. These influence matrices are used to evolve the solution from one time-step to the next. This procedure is outlined in appendix A for the case of piecewise constant and linear basis functions resulting in the evolution eq. (A.2). In order to obtain accurate solutions in the vicinity of a boundary point or an active site when desorption is present, it is necessary to use an asymptotic expansion of the boundary influence matrices. The required asymptotic expansions are given in appendix B.

3.3. Time marching

We exploit the Volterra form of the time integrals in (3.3) to construct the following time-marching scheme. The solution is carried from one time level t_j to the next $t_{j+1} = t_j + \Delta t_j$ by using (3.3) in which $t = \Delta t_j$ and the solution values at time t_j are regarded as initial values, i.e., $u^0(x) = u(x, t_j)$. Depending on the prescribed boundary conditions we solve (3.3) for $\partial u(x_i)/\partial \xi$ $i = 0, N$ when $u(x_i)$ are given, or for $u(x_i)$ $i = 0, N$ when $\partial u(x_i)/\partial \xi$ are given. Eq. (3.3) is then used to generate $u(x, t_{j+1})$, which can in turn be used as initial data for the next step.

If we assume that all the time-steps are the same size, then a substantial computational saving can be achieved by a priori generation and storage of the required influence matrices mentioned above. Thus the discretized BE equations can be used to advance the solution by a procedure that involves mainly matrix multiplication (i.e., explicitly). Only terms involving the boundary unknowns and active sites have to be solved at every time-step (i.e., treated implicitly). In fact, numerical experiments suggest that instead of solving the non-linear equations for $u(x_l, t)$ $l = 1, \ldots, L$ at the L active sites, it is reasonable to assume $u(x_l, t_i + \Delta t) = u(x_l, t_i)$ provided $\Delta t \| (\partial R_l/\partial u)$

$\times(\partial u/\partial t)\| \ll \| R_i(u)\|$ at t_j. This assumption essentially allows non-linear effects to be treated explicitly too. This procedure will be outlined in the next two subsections.

3.4. Solution of the non-linear equations associated with the active sites

There are a number of different strategies that could be used to solve the $S\times(Q-1)\times(L)$ non-linear equations for the unknowns $u(x_{r_l}, t_j + t^b)$ $\{r_l\}_{l=1}^{L}$; $2 \le b \le Q$ that appear in eq. (A.2). One such technique involves an iterative predictor–corrector sequence. Initially we assume that $u(x_{r_l}, t)$ is constant over the time-step Δt. Using these values of u on the right-hand side of (A.2), we can calculate new values of $u(x_{r_l}, t_j + t^b)$. These values are in turn substituted on the right-hand side of (A.2) and so on. This is an example of the general iterative method for solving non-linear equations [16]. In order to consider the convergence of such a scheme, assume the special case in which there is only one species (so $S = 1$), only one active site (so $L = 1$), and we have approximated u by a linear function over $[0, \Delta t]$ so that $Q = 2$. If we assume that the active site is remote from the boundaries then a sufficient condition for the convergence of the iterative scheme when applied to the single non-linear equation is that

$$\left|\int_0^{\Delta t} G(0, \Delta t - \tau) R'\big(T^1(\tau)u^1 + T^2(\tau)u^2\big)T^2(\tau)\,\mathrm{d}\tau\right| < 1,$$

where the shape functions T^k are defined in appendix A. If we assume that $R \in C^2$ we can show using integration by parts that:

$$\int_0^{\Delta t} G(0, \Delta t - \tau) R'\big(T^1(\tau)u^1 + T^2(\tau)u^2\big)T^2(\tau)\,\mathrm{d}\tau$$

$$\sim \frac{2}{3}\left(\frac{\Delta t}{\pi D}\right)^{1/2} R'(u^2) + \mathrm{O}(\Delta t^{3/2}), \quad \Delta t \to 0,$$

Thus the iterative scheme can always be made to converge by choosing Δt sufficiently small.

We now consider a scheme that assumes that the solution u at each active site is constant over the time-step $[0, \Delta t]$. This amounts to taking only the first step in the above iterative algorithm. This procedure is extremely attractive from a computational point of view as the solution is then taken from one time-step to the next in an explicit fashion and no non-linear equations have to be solved. A variant of this scheme is to calculate the effect of the integrals:

$$\int_{x_0}^{x_N} Gu^0\,\mathrm{d}\xi, \quad \int_0^{\Delta t} \sum_{x_0, x_N} GD\frac{\partial u}{\partial \xi} - \frac{\partial G}{\partial \xi} Du\,\mathrm{d}\tau$$

(assuming u and $\partial u/\partial \xi$ are constant over $[0, \Delta t]$), and

$$\int_0^{\Delta t}\int_{x_0}^{x_N} Gf\,\mathrm{d}\xi\,\mathrm{d}\tau$$

in (3.3) evaluated at each of the active sites x_{r_l}. This estimate of $u(x_{r_l}, t_{j+1})$ is then used to obtain a more accurate approximate of the integral $\int_0^{\Delta t} GR_l(u(x_l, \tau)\, d\tau$ using linear interpolation. This is essentially the piecewise linear Caratheodory iteration scheme used by Peirce et al. [12] in the analysis of convergence of BE approximations in the non-linear regime. The results of this analysis are summarized in the next section. This explicit scheme will be used for the numerical examples given in this paper. Naturally this algorithm could be improved by using the iteration scheme outlined above or by employing a Newton–Raphson scheme – with a concomitant overhead in computing costs.

3.5. Convergence properties of piecewise polynomial BE approximants

In this section we summarize the convergence properties of BE approximations based on the piecewise polynomial collocation schemes that were described in section 3.2 and appendix A. The analysis, which was performed by the current authors [12], provides a theoretical framework for resolving meshing issues such as the appropriate size of time-stepping.

In the absence of active sites it is possible to identify a dimensionless mesh parameter the magnitude of which determines the performance of a given mesh. BE meshes based on piecewise constant and piecewise linear collocation are shown to be *conditionally* convergent. Surprisingly, this loss of convergence occurs when the size of time-steps is small relative to spatial meshing and manifests itself in the form of excess diffusion. The magnitude of this excess diffusion can be predicted precisely by the theory. On the other hand, BE schemes based on piecewise quadratic collocation are unconditionally convergent and do not display any excess diffusion. Another surprising result is that for all three schemes time-steps can be made as large as desired without any instability occurring, provided that the degree of boundary interpolation is sufficient to prevent a degradation in accuracy.

In the case that active sites are present with non-linear reactions taking place, the issue of convergence is more complicated. By considering a model problem, it is possible to prove that the piecewise linear Caratheodory iterates outlined in section 3.4 do converge to a solution on a finite time horizon. The extent of the convergence region depends on how long the solution is guaranteed to exist. This analysis provides a theoretical justification for the use of the piecewise linear collocation scheme in a non-linear environment.

4. Numerical examples

In this section we present BE solutions for four different localized reaction diffusion problems. The first of these is the so-called distributed Lotka–Volt-

erra system, which has been chosen as it provides a stringent test of the stability of the numerical technique. The second system comprises the Prigogine–Lefever reaction, which is assumed to occur at each defect in a periodic array of defects. The parameters of this system are chosen so that marginal stability oscillations occur in the vicinity of an equilibrium solution. These marginal stability oscillations were first identified by Bimpong-Bota et al. [6] using linear stability analysis. The remaining two problems consider the effects of defect structures on the desorptive processes that occur on catalytic surfaces. In another paper [2], the current authors have given a detailed analytic and numerical account of the effect of defect locations on the balance between the steady state desorptive processes that occur on catalytic surfaces *assuming time independent adsorption*. In the third problem of this section we investigate the effect of dynamic pulsing of the adsorption level on the competitive behavior between defects, which was identified for static adsorption levels. The competitive behavior is shown to persist for the case of periodic pulsing of the surface. In the fourth problem we consider the effect of defect locations on the desorption processes for a more complex three-species model. Similar competitive phenomena are demonstrated in this more complex environment. These latter two examples illustrate the pervasiveness of these competitive/cooperative phenomena associated with the defects on catalytic surfaces. In addition, these examples illustrate the stability of the BE technique and its usefulness in analyzing the physical phenomena associated with defects structures.

4.1. Distributed, diffusion-coupled Lotka–Volterra system

We consider the numerical solution of the following system of partial differential equations with non-linear auxiliary conditions:

$$\frac{\partial u_i}{\partial t} = D_i \frac{\partial^2 u_i}{\partial x^2} - \Omega_i u = 0, \qquad i = 1, 2, \quad x \in [-L, L], \tag{4.1a}$$

$$u_i(x, 0) = 1, \qquad i = 1, 2, \tag{4.1b}$$

$$-D_1 \frac{\partial u_1}{\partial x} = \alpha u_1 \Big|_{x=-L}, \quad -D_1 \left[\frac{\partial u_1}{\partial x}\right] = -\beta u_1 u_2 \Big|_{x=0}, \quad \frac{\partial u_1}{\partial x} = 0 \Big|_{x=L}, \tag{4.1c}$$

$$\frac{\partial u_2}{\partial x} = 0 \Big|_{x=-L}, \quad -D_2 \left[\frac{\partial u_2}{\partial x}\right] = \beta u_1 u_2 \Big|_{x=0}, \quad D_2 \frac{\partial u_2}{\partial x} = -\gamma u_2 \Big|_{x=L}, \tag{4.1d}$$

where the jump condition form defined in (2.3) has been used and α, β and γ are all non-negative constants. Eqs. (4.1) represent a Lotka–Volterra system in which the linear source and sink terms are located at the two boundaries of the domain, and the non-linear predator–prey interaction occurs at a single active site. Bulk diffusion couples the active site with the source and sink points at

the boundaries. This system has been chosen as it provides a stringent test of the stability of the numerical scheme, since for the given initial condition the numerical solution is required to traverse a large region near the axis $u_2 = 0$ without moving into the unphysical region $u_2 < 0$. Another interesting feature of this model is that it is an oscillator driven by diffusion. The model represents the introduction of species 1 at $x = -L$ from a bath of material, while species 2 is prevented from escaping from this point. At the defect $x = 0$, species 1 and 2 are converted to species 2 according to $S_1 + S_2 \rightarrow 2S_2$. At the boundary $x = L$, species 2 flows into a bath of material while species 1 is prevented from escaping at this point. The whole process is coupled by diffusion. Desorption of both species is included in the model.

4.1.1. Steady states of the distributed Lotka–Volterra system

By solving the system (4.1) with $\partial u_i/\partial t = 0$ we obtain the steady state solutions of (4.1):

$$u_1(x) = \begin{cases} u_1(0)\left[\cosh(\omega_1 x) - q_1 \sinh(\omega_1 x)\right], & x \le 0, \\ u_1(0)\cosh\left[\omega_1(x-L)\right]/\cosh(\omega_1 L), & x > 0, \end{cases} \tag{4.2a}$$

$$u_2(x) = \begin{cases} u_2(0)\cosh\left[\omega_2(x-L)\right]/\cosh(\omega_2 L), & x \le 0, \\ u_2(0)\left[\cosh(\omega_2 x) - q_2 \sinh(\omega_2 x)\right], & x < 0, \end{cases} \tag{4.2b}$$

where

$$\omega_i = (\Omega_i/D_i)^{1/2},$$

$$q_1 = \frac{-D_1\omega_1 \sinh(\omega_1 L) + \alpha \cosh(\omega_1 L)}{D_1\omega_1 \cosh(\omega_1 L) - \alpha \sinh(\omega_1 L)},$$

$$q_2 = \frac{-D_2\omega_2 \sinh(\omega_2 L) + \gamma \cosh(\omega_2 L)}{D_2\omega_2 \cosh(\omega_2 L) - \gamma \sinh(\omega_2 L)},$$

and

$$(u_1(0),\ u_2(0)) = (0, 0), \tag{4.3a}$$

or

$$(u_1(0),\ u_2(0)) = \left(\frac{D_2\omega_2\left[q_2 + \tanh(\omega_2 L)\right]}{\beta},\ \frac{D_1\omega_1\left[q_1 - \tanh(\omega_1 L)\right]}{\beta}\right) \tag{4.3b}$$

$$\xrightarrow{\omega_i \to 0} \left(\frac{D_2/\beta}{D_2/\gamma + L},\ \frac{D_1/\beta}{D_1/\alpha - L}\right). \tag{4.3c}$$

We notice that in the limit $D_i \rightarrow \infty$ the steady state (4.3c) reduces to that of the standard non-distributed Lotka–Volterra ODE system. This is in agreement with physical intuition, since the time-scale on which the diffusion processes take place is in this case much smaller than that of the reaction processes. The reaction processes then take place as if they were all located at one point.

4.1.2. Stability of the distributed Lotka–Volterra system

We consider a small perturbation $v_i^0(x)$ to the steady states given in (4.2) and let $v_i(x, t)$ be the subsequent evolution of this initial perturbation. The equation governing the evolution of $v_i(x, t)$ can be obtained by perturbation of (4.1) and can be seen to be identical to (4.1) except for the jump conditions at $x = 0$ which are of the form:

$$-D_i\left[\frac{\partial v_i}{\partial x}\right] = \sum_{j=i}^{2} J_{ij} v_j(0), \tag{4.4}$$

where

$$J = \begin{bmatrix} -\beta u_2(0) & -\beta u_1(0) \\ \beta u_2(0) & \beta u_1(0) \end{bmatrix}.$$

We use Laplace transforms to analyze the growth or decay of the perturbation $v_i(x, t)$. We take the Laplace transform of (4.1) with u_i replaced by v_i and replace the jump conditions at $x = 0$ in (4.1c and 4.1d) by the jump conditions (4.4). The stability of the system is determined by the roots $s^* \in \mathbb{C}$ of the transcendental equation:

$$\det\left[\delta_{ij}\psi_j(s^*) - J_{ij}\right] = 0, \tag{4.5}$$

where

$$\psi_1(s) = D_1\omega_1\left[\frac{D_1\omega_1 \sinh(2\omega_1 L) - \alpha}{D_1\omega_1 \cosh^2(\omega_1 L) - \alpha \sinh(\omega_1 L)\cosh(\omega_1 L)}\right],$$

$$\psi_2(s) = D_2\omega_2\left[\frac{D_2\omega_2 \sinh(2\omega_2 L) + \gamma}{D_2\omega_2 \cosh^2(\omega_2 L) + \gamma \sinh(\omega_2 L)\cosh(\omega_2 L)}\right]$$

and

$$\omega_i = \left(\frac{s + \Omega_i}{D_i}\right)^{1/2}.$$

We notice that in the limit $D_i \gg 1$

$$\psi_1(s) \sim \frac{2L(s + \Omega_1) - \alpha}{1 - \alpha L/D_1},$$

$$\psi_2(s) \sim \frac{2L(s + \Omega_2) - \gamma}{1 + \gamma L/D_2}.$$

If we also assume $\Omega_1 = \Omega_2 = \Omega$, then (4.5) reduces to

$$4L^2(s^* + \Omega)^2 + 2L(s^* + \Omega)\left[\gamma - \alpha - \left(1 - \frac{\alpha L}{D_1}\right)J_{11} - \left(1 + \frac{\gamma L}{D_2}\right)J_{22}\right]$$

$$- \alpha\gamma - J_{11}\gamma\left(1 - \frac{\alpha L}{D_1}\right) + J_{11}\alpha\left(1 + \frac{\gamma L}{D_2}\right) \approx 0. \tag{4.6}$$

We use the steady states ((4.3a) and (4.3c)) to evaluate J_{ii} and conclude from (4.6) that:

(i) when $(u_1(0), u_2(0)) = (0, 0)$:

$$s^* = -\Omega + \alpha \quad \text{or } s = -\Omega - \beta; \tag{4.7a}$$

(ii) when $(u_1(0), u_2(0)) \approx ((\gamma/\beta)/(1 + \gamma L/D_2), (\alpha/\beta)(1 - \alpha L/D_2))$:

$$s^* = -\Omega \pm \frac{i\sqrt{\gamma\alpha}}{2L}. \tag{4.7b}$$

When $\Omega = 0$ it can be seen from (4.7a) that the trivial solution is unstable,

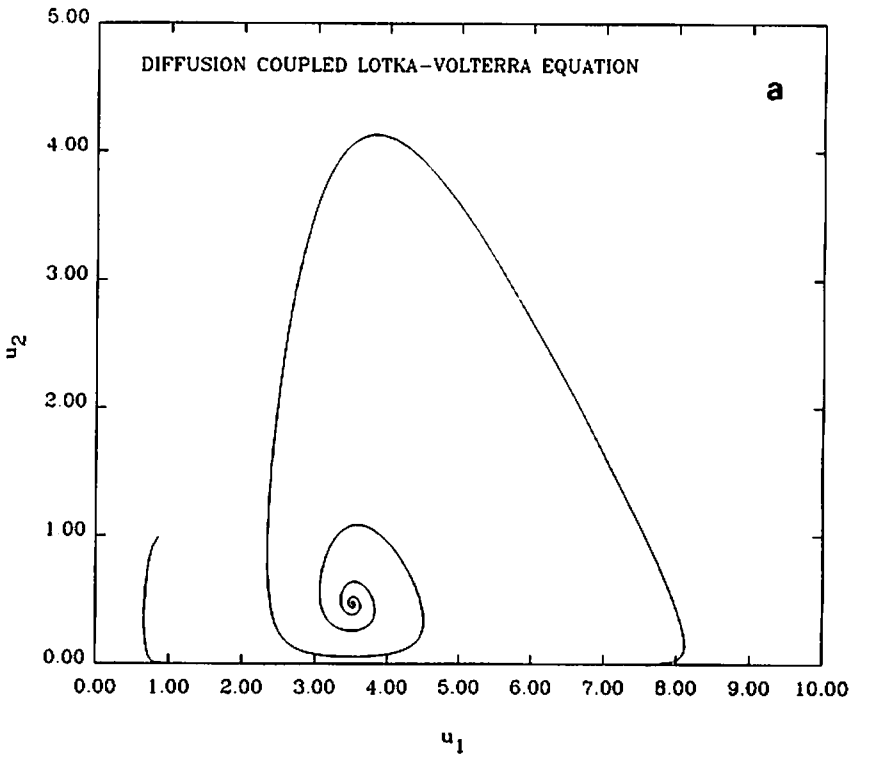

Fig. 1a. The evolution in the phase plane of the concentrations at the defect site for the diffusion coupled Lotka–Volterra equation. This example has been chosen as it provides a stringent test of the stability of the numerical algorithm since a large portion of the region close to the axis $u_2 = 0$ has to be traversed without the solution moving into the unphysical region $u_2 < 0$. The stable spiral behavior is consistent with the linear stability analysis and the steady state achieved by the numerical algorithm after $t = 100.0$ agrees well with the exact steady state solution at the active site. It is interesting to note that the trajectory comes reasonably close to itself in the region $3.0 \leq u_1 \leq 4.0$ and $0.0 \leq u_2 \leq 0.2$ and then subsequently moves to very different parts of the phase plane. This is not some sort of instability of the problem but a reflection of the very different spatial structure of the solutions associated with these two parts of the trajectory. This can be seen in fig. 1b.

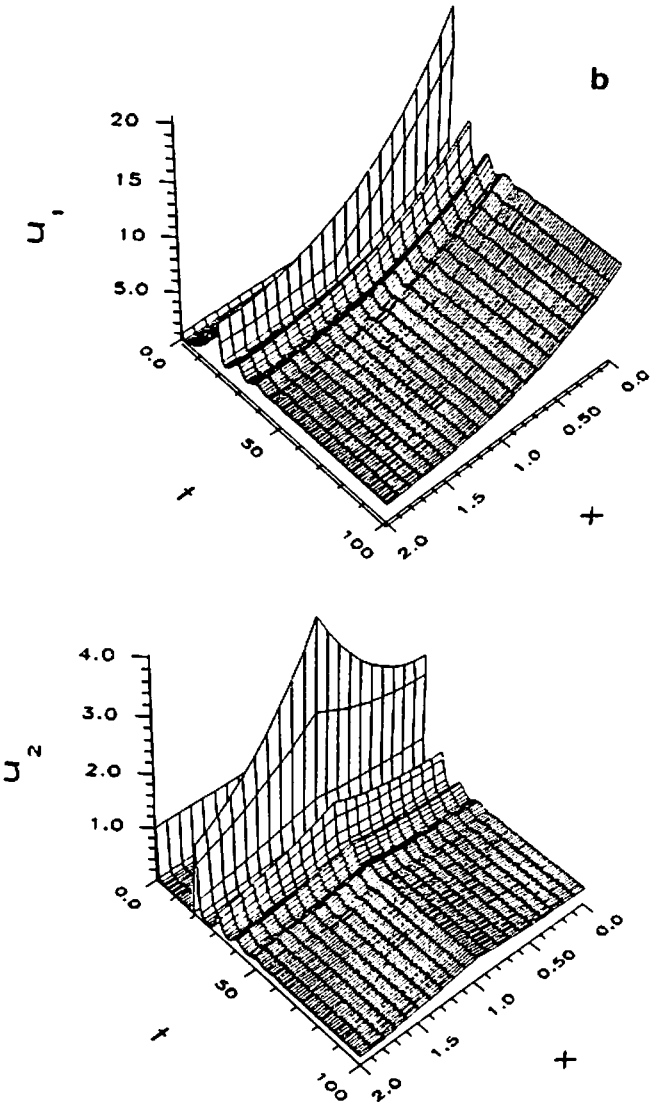

Fig. 1b. The space-time distribution of the concentration u_1 and u_2. The change in the spatial distribution of the concentrations with time can be seen clearly. The entrainment of the oscillations throughout the domain by that at the active site can also be observed.

whereas (4.7b) shows that the system will perform marginal oscillations in the vicinity of the second steady state defined by (4.3c).

When $\Omega > 0$ it can be seen from (4.7a) that the trivial solution is a stable node provided $\Omega > \alpha$; whereas (4.7b) shows that the second steady state defined by (4.7b) will be a stable spiral.

4.1.3. Discussion of results

Fig. 1a plots the evolution in the phase plane of the concentrations at the active site obtained by the BE technique. An accurate spatial discretization of the BE equations using quadratic interpolation and 60 mesh points has been used. The size of time-step was $\Delta t = 0.01$. The parameters used in this model were $D_1 = D_2 = 2.0$; $\alpha = \beta = \gamma = 1.0$, $L = 1.0$ and $\Omega = 2.0$. The steady state concentrations at the active site obtained from (4.3b) are $(u_1(0), u_2(0)) = (3.524, 0.477)$ which can be seen to agree well with the numerical solution (3.524, 0.471) after an elapsed time of $t = 100.0$. The stable spiral behavior is consistent with that predicted in (4.7b).

It is striking to note the large portion of the region close to the line $u_2 = 0$ that the numerical solution is able to traverse without moving into the unphysical region $u_2 < 0$. What is also interesting is the closeness of the trajectories in the region $3.0 \leq u_1 \leq 4.0$ and $0 < u_2 \leq 0.2$. Here two neighboring points move large distances from one another as time progresses. This would seem to indicate some sort of instability of the system. However, it should be emphasized that we are only looking at the phase portrait at the active site, in which the two neighboring points are in fact associated with solutions with very different spatial structures. This can be seen clearly in fig. 1b in which the space–time evolution of the concentrations is plotted. An interesting feature of these space–time plots is the way in which the damped oscillations throughout the domain follow the oscillations at the active site.

4.2. Marginal oscillations of the Prigogine–Lefever reaction which occurs at defects on a periodic lattice

Bimpong-Bota et al. [6] considered a periodic lattice of defects located at $x_n = 2nL$; $n = 0, \pm 1, \ldots$. At each of these defects the Prigogine–Lefever reaction:

$$R_1(u) = \lambda\left(A - Bu_1 + u_1^2 u_2 - u_1\right), \tag{4.8a}$$

$$R_2(u) = \lambda\left(Bu_1 - u_1^2 u_2\right), \tag{4.8b}$$

is assumed to occur. The defects are coupled by diffusion of the species as described by (2.1) and it is assumed that no bulk desorption or adsorption occurs so that the steady state solutions are constant functions. They show using linear stability analysis that the marginal oscillations about the steady state $(u_1^*, u_2^*) = (A, B/A)$ of the Prigogine–Lefever system are given by the roots β and B of the equation:

$$\psi(\mathrm{i}\beta) = \tfrac{1}{2}\lambda(B-2) + \mathrm{i}\tfrac{1}{2}\lambda(4B - B^2)^{1/2}, \tag{4.9}$$

where $\psi(s) = 2(Ds)^{1/2} \tanh[(s/D)^{1/2}L]$ and $A = 1$. In many physical systems reaction terms of the form (4.8) are the object of some criticism on physical

grounds due to the third-order terms. These reactions are unlikely to occur in a bulk fluid medium since they represent the joint probability that two atoms of species 1 and a single atom of species 2 will be at the same place at the same time. However, in the context of localized reactions at defects, it can be argued that this type of reaction is more likely to occur owing to the fact that a defect structure will form a collection point for many reagents.

Using the BE technique the localized Prigogine–Lefever system was modelled in the vicinity of the steady state $(u_1^*, u_2^*) = (1.0, 2.8227)$. The choice of parameters in this case was $\lambda = 1.0$, $D_1 = D_2 = 1.0$, $L = 2.5$. The critical values of β and B for this set of parameters, determined from the complex transcendental equation (4.9), are $\beta_c = 0.1146$ and $B_c = 2.8227$. Exploiting the periodicity of the problem we considered a single defect located at the midpoint $x = 2.5$ of the interval [0, 5] and assumed zero flux boundary conditions. The BE equations were solved using quadratic interpolation and 60 mesh points and the size of time-step was $\Delta t = 0.01$.

In fig. 2a the evolution in the phase plane of the concentrations at the defects are plotted for the solutions with the following spatially uniform initial conditions:

(i) $(u_1^0, u_2^0) = (1.000, 2.820)$;
(ii) $(u_1^0, u_2^0) = (1.020, 2.800)$;
(iii) $(u_1^0, u_2^0) = (1.040, 2.777)$;
(iv) $(u_1^0, u_2^0) = (1.000, 2.760)$.

We observe that the concentrations at the defect rapidly approach a stable cycle for trajectories (i) and (ii). This is consistent with the marginal stability oscillations predicted by the linear stability analysis. For trajectories (iii) and (iv) a dissipative spiral behavior occurs. This dissipative behavior is due to non-linear effects that occur when large perturbations are made to the steady state. These effects are neglected in the linear stability analysis. By comparing trajectories (iii) and (iv) it can be seen that the rate of dissipation depends on the magnitude of the initial perturbation.

Another interesting phenomenon that can be seen clearly in the case of trajectory (ii) is a rapid evolution from the initially spatially uniform perturbed state to a state with the appropriate spatial distribution for marginal stability oscillations. This explains the outward spiral behavior observed in the initial part of trajectories (ii), (iii) and (iv).

As an illustration of the spatial redistribution effect, trajectory (ii) of fig. 2a is plotted (solid line) in fig. 2b together with the corresponding trajectory (dotted line) of the concentrations at $x = 1.25$ located midway between the defect and the boundary. The two trajectories start at the same point $(u_1^0, u_2^0) = (1.020, 2.800)$ (due to the spatially uniform initial conditions) and move into different cycles.

We have seen that the BE technique is able to capture the marginal stability oscillations in a stable fashion and to establish dissipative behavior when

initial perturbations are sufficiently large for non-linear effects to become significant. From a physical point of view these stable cycles are particularly interesting in view of the fact that third-order reaction terms are more likely to occur at defect structures that form collection points for the reagents.

4.3. A continuum model of reactive trapping by defects

Assuming a constant adsorption rate the current authors [2] have given a detailed analytic and numerical account of the effect of defect locations on the steady state desorptive processes that occur on catalytic surfaces. A class of reactive trapping models was considered in which defects act as sinks of

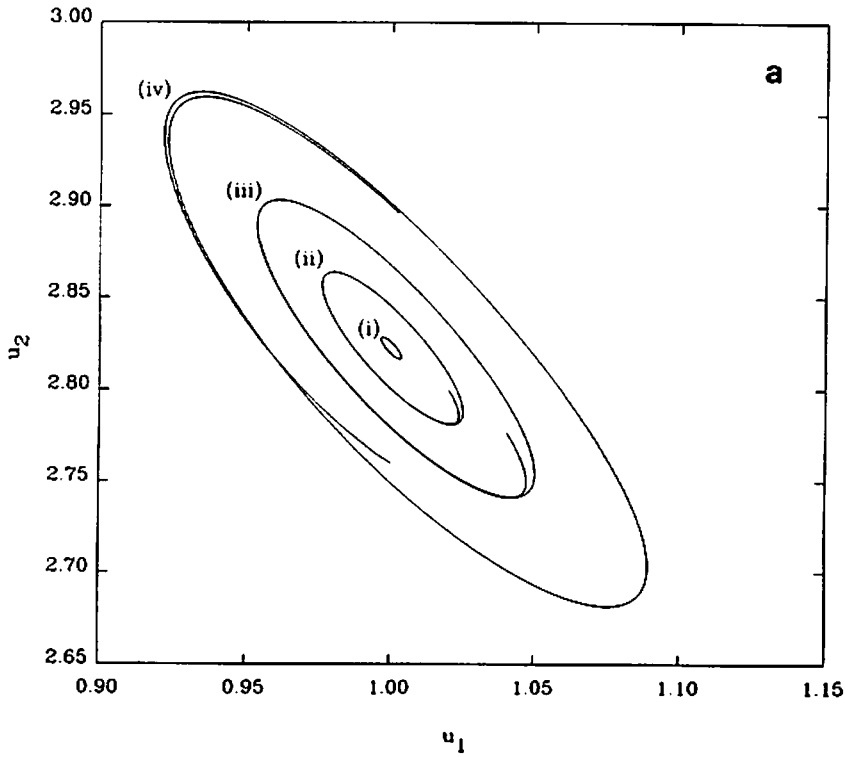

Fig. 2a. The evolution in the phase plane of the concentrations at the defect for four distinct spatially uniform initial perturbations to the steady state (u_1^*, u_2^*). The marginal stability oscillations predicted by linear stability theory occur for the smaller two perturbations to the steady state (i) and (ii). However, when size of the initial perturbation is increased, a dissipative spiral behavior occurs due to the effect of the non-linear terms that are neglected in the linear stability theory. Another interesting phenomenon that can be observed for trajectories (ii), (iii), and (iv) is the rapid evolution from an initially spatially uniform state to a state with the appropriate spatial distribution for marginal stability oscillations. This spatial redistribution is demonstrated in fig. 2b for trajectory (ii).

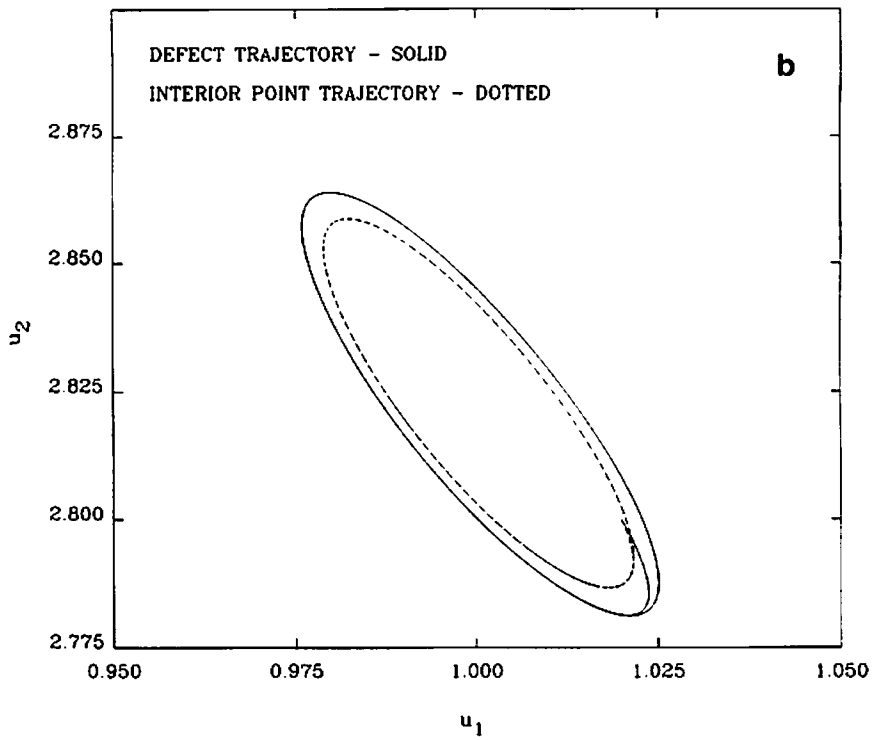

Fig. 2b. The evolution in the phase plane of the concentrations at the defect (solid line) that is located at $x = 2.5$ and at an interior point $x = 1.25$ (dotted line) for the initial perturbation (ii). Since the initial perturbation is spatially uniform, the two trajectories start in the same place but end up on different orbits, which demonstrates the spatial redistribution to the marginal oscillation states.

material that ultimately desorbs as a chemical product. Other features included in that model were enhanced reactivity with concentration and saturation effects. The effect of defect locations on desorptive processes were analyzed by considering symmetry-breaking perturbations to a periodic array of defects. Two regimes of desorption were identified depending on the level of adsorption to the surface and the defect spacing:

(i) Competitive: defects that are moved closer together by the perturbation compete for material that reduces the trapping efficiency of the defects. The bulk (i.e. non-defect) desorption rate increases.

(ii) Cooperative: defects that are moved closer together by the perturbation in this regime act cooperatively to reduce the saturation level locally. This enhances the trapping efficiency of the defect lattice and reduces the bulk desorption rate.

These interesting competitive/cooperative desorptive phenomena were investigated in the steady state limit assuming constant adsorption to the surface.

In this section we explore the effect of dynamic adsorptive pulsing on these competitive/cooperative phenomena. We assume that the pulsing is in the form of a square wave in which the time period of a single pulse is T. We assume that we start with a periodic lattice of defects located at $x_n = 2nL$, $n = 0, \pm 1, \ldots, N$ within the interval $[-r, r]$. The surface containing these line defects is then pulsed and the desorption rate

$$\mathscr{D} = \frac{\Omega}{2r} \int_{-r}^{r} u \, dx \tag{4.10}$$

is determined. The defects are then subjected to finite random spatial perturbations and the pulsing process is repeated. The change in desorption rate $\mathscr{D}$ due to the perturbation of the uniformly distributed defects provides a measure of how the balance between the bulk desorption and the desorptive effect of the defects is altered by changing the locations of the defects. We assume that there is a single species that is being trapped at the defects according to the reactive trapping model:

$$R(u) = -(1-u)u \tag{4.11}$$

and that the bulk diffusion, desorption and adsorption processes are governed by (2.1) in which $D = 1.0$, $\Omega = 2.0$ and

$$f(t) = 2S(t)$$

where

$$S(t) = \begin{cases} 1, & nT \le t < (n+\frac{1}{2})T, \\ 0, & (n+\frac{1}{2})T \le t < (n+1)T, \end{cases} \qquad n = 0, 1, \ldots .$$

The results of this analysis are contrasted with those in which a constant adsorption level $f = 1.0$ is used. This corresponds to a uniform adsorption level that delivers the same average amount of material to the surface. Reference to this uniform adsorption function allows us to use theory developed [2] previously, assuming uniform adsorption, to identify possible regimes of competitive behavior in the dynamic case. In particular if $L = 0.1$ then the static theory [2] predicts competitive trapping behavior between perturbed defects, which will cause the bulk desorption rate to increase when a uniform array of defects is perturbed.

In the laboratory pulsed modulation of the incident flux would be beneficial for various reasons including the introduction of a laboratory controlled time-scale. Resonance effects might be expected for $T \sim L^2/D$, the characteristic time-scale of diffusion on the lattice or other natural time-scale of the system. If $T \ll L^2/D$ then by rescaling of variables in (2.1) the diffusion coefficient can be shown to be of order $\epsilon = TD/L^2$. The diffusion process on the surface is in this case extremely weak and the points throughout the

surface will behave to first order as if they were decoupled. The decoupling implies that this limit is not very interesting from the point of view of competitive behavior between defects. We shall therefore not pursue this limiting case. In this section we consider dynamic pulsing at two different time-scales $T = 0.02 \sim L^2/D = 0.01$ and $T = 0.8 \gg L^2/D$.

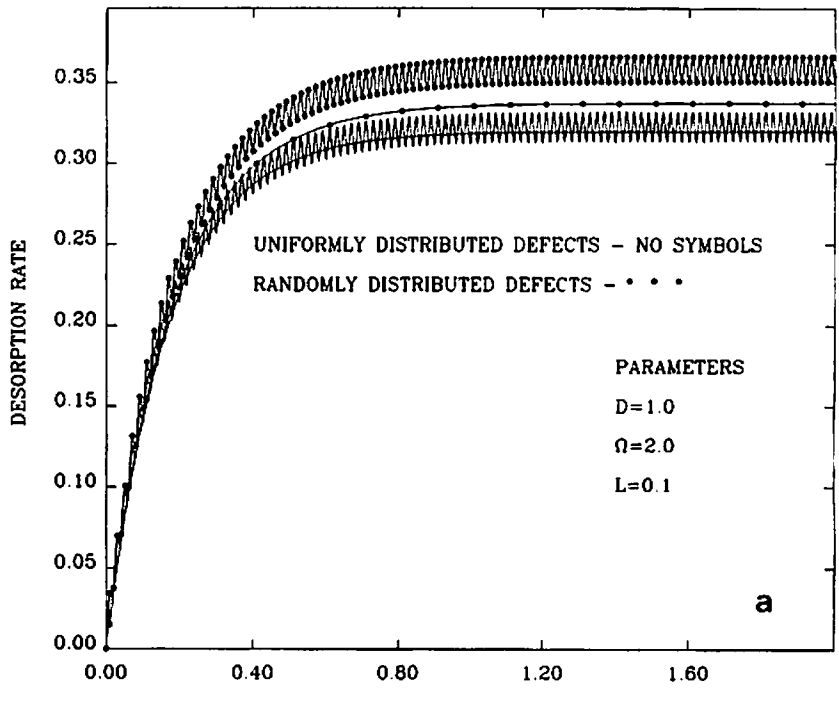

Fig. 3a. The time evolution of the desorption rate $\mathscr{D}$ for 10 defects spaced over the interval [0, 2.0], assuming that reactive trapping given by (4.11) occurs at the defects. The desorption rate provides a measure of the balance between the bulk desorption rate and the desorption due to the reactive trapping that occurs at defects. Two different distributions of defects are considered: a uniform distribution (denoted by functions with no symbols) and a random distribution of the same number of defects (denoted by functions with a solid circle). Two types of adsorption are applied to the surface. In the first type of adsorption, the surface is pulsed with a square wave pulse having a period $T = 0.02$, while the characteristic diffusion time-scale of the defect lattice is $L^2/D = 0.01$. In the second type of adsorption, the surface is supplied with the same average amount of material as in the dynamic case, but at a uniform rate. In both the static case and the dynamic case the bulk desorption rate increases as a result of perturbing the uniformly distributed defects. This is due to competitive behavior between the defects that are moved closer by the perturbation, which results in a decrease in the trapping efficiency of the defects as a whole and an increase in the bulk desorption rate. Therefore, the competitive behavior that has been established for static adsorption levels persists when the surface is pulsed periodically. It is interesting to note that the mean increase in the desorption rate is larger in the dynamic case than in the static case.

In the case of the short time-scale $T = 0.02$ the BE equations are solved on [0, 2] using quadratic interpolation and 90 spatial mesh points. The size of the time-step was $\Delta t = 0.001$. It should be noted that the convergence theory discussed in section 3.5 is useful in this case for deciding on an appropriate meshing strategy. If piecewise constant or piecewise linear interpolation is used for time-steps as small as this, then to avoid the significant numerical diffusion described in section 3.5, we would require at least 400 mesh points. Since the quadratic interpolation scheme was shown not to suffer from this problem it was chosen for the purposes of this example. In the case of the long time-scale the same spatial meshing was used while the size of the time-step was 0.01.

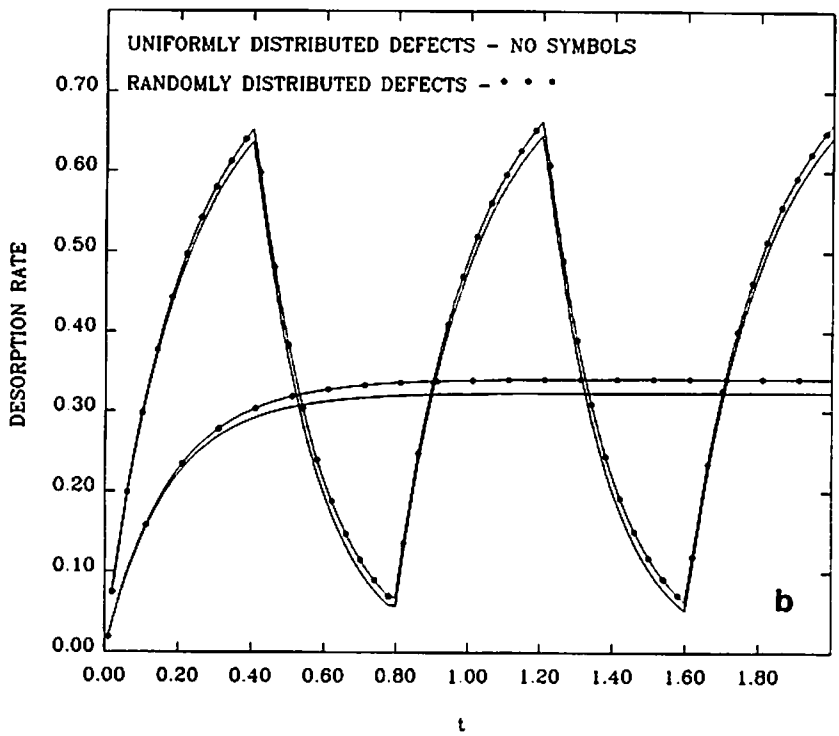

Fig. 3b. The time evolution of the average desorption rate $\mathscr{D}$ is plotted as is done in fig. 3a. However, in this case the period of the pulsed adsorption is $T = 0.8$, which is much larger than the characteristic diffusion time scale $L^2/D = 0.01$. The results for constant adsorption which delivers the same amount of material to the surface are also plotted. The desorption response of the system to square wave pulsing is in the form of relaxation oscillations due to the larger time-scale of the pulsing. No phase lag is observed because of the rapid diffusion time-scale. In both the static case and the dynamic case the bulk desorption rate increases as a result of perturbing the uniformly distributed defects. This demonstrates that the competitive behavior persists in this regime of periodic pulsing.

In fig. 3a the time evolution of the desorption rate $\mathscr{D}$ is plotted for the case of 10 defects uniformly distributed over the interval [0, 2.0] so that $L = 0.1$. These defects are then each subjected to a finite random perturbation and the adsorption process is repeated. Results are shown for pulsed adsorption with period $T = 0.02$ and a constant rate of adsorption to the surface. According to constant adsorption theory [2], the defects are for this level of adsorption in the competitive regime, so that perturbations to the uniform lattice are expected to increase the bulk desorption rate. We observe that the competitive behavior persists when the surface is pulsed and that the mean increase in bulk desorption rate for the pulsed surface is larger than that for the surface supplied with the same amount of material at a uniform rate. It is interesting to note the sawtooth structure of the oscillations in the desorption rate. This piecewise linear behavior can be explained by looking at the initial linear increase of the desorption rate $\mathscr{D}$ in the time interval [0, 0.2] for the constant adsorption cases in fig. 3a. The time-scale for non-linear increase of $\mathscr{D}$ to occur can also be read from these plots. In particular we would expect a non-linear increase of $\mathscr{D}$ to occur on the time-scale $T = 0.8$. This relatively simple response of the system is probably due to the fact that we are considering only a one species system. In a more complex multiple species problem a variety of time-scales are likely to occur. This would certainly make the response function more complex when the pulsing has a period close to one of these time-scales.

In fig. 3b the time evolution of the desorption rate $\mathscr{D}$ for uniformly and randomly spaced defects is plotted for pulsed adsorption with a period $T = 0.8$, and for constant adsorption at a level that delivers the same average amount of material to the surface. As predicted above, a non-linear response function is observed which is in the form of a sequence of relaxation oscillations. There is no phase lag in the response to the pulse owing to the faster diffusion time-scale. As was the case in fig. 3a the average desorption rate $\mathscr{D}$ increases when the uniformly distributed defects are perturbed. Thus competitive behavior between the defects persists in this regime of adsorption.

This example serves to demonstrate the interesting features that can result from an analysis of the continuum model of defect structures. The overlay feature of the BE technique is particularly useful when the effects of randomly spaced defects are included in the analysis.

4.4. Competitive behavior in a three-species reaction occurring at defects

In this section we demonstrate that the competitive behavior of defects is not restricted to the simple reactive trapping model considered in section 4.3. We use the same procedure adopted in the previous section to investigate the effect of defect locations on the balance between the desorptive processes that occur on surfaces with defects. However in this case we consider a more complex three-species model with saturation effects.

We assume that we start with a periodic array of defects located at $x_n = 2nL$, $n = 0, \pm 1, \ldots$, which are then subjected to finite random perturbations. We assume that three species are present on the surface and that bulk diffusion, adsorption and desorption processes are governed by (2.1) in which $D_1 = D_2 = D_3 = 1.0$, $\Omega_1 = \Omega_2 = \Omega_3 = 2.0$ and $f_1 = 1.0$, $f_2 = 2.0$ and $f_3 = 0.0$. We assume that the same reaction occurs at each of the defects in which the components of the reaction function $\boldsymbol{R}(\boldsymbol{u})$ in (2.1) are given by:

$$R_1(u_1, u_2, u_3) = k_1(s_2 - u_2)u_1,$$
$$R_2(u_1, u_2, u_3) = k_2(s_1 - u_1)u_2, \tag{4.12}$$
$$R_3(u_1, u_2, u_3) = k_3 u_1 u_2.$$

In (4.12) species 1 and 2 collect at the defects and react to form species 3. The

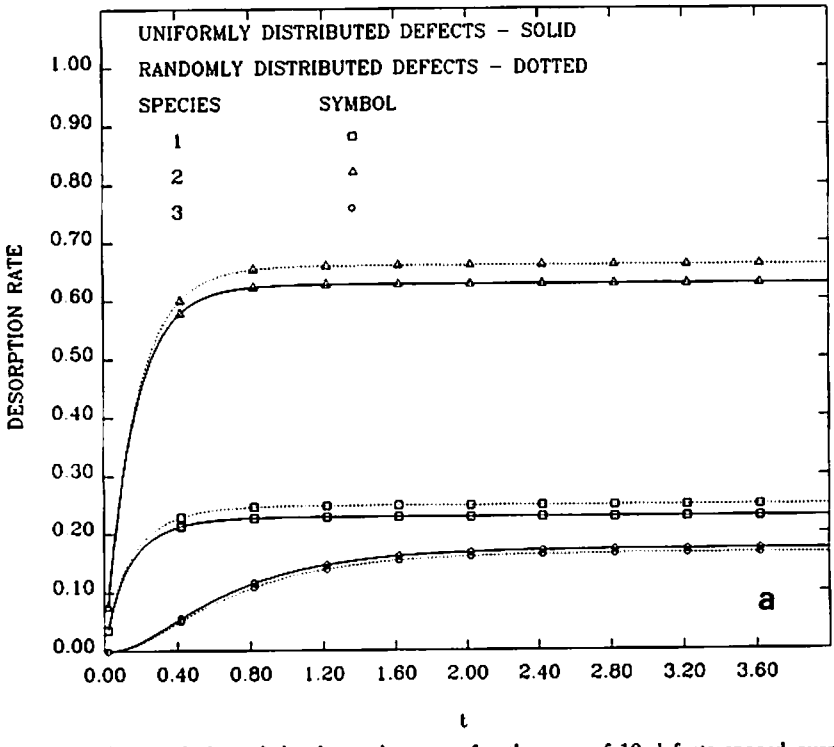

Fig. 4a. The time evolution of the desorption rates for the case of 10 defects spaced over the interval [0, 2.0], assuming that the three species reaction (4.12) occurs at the defects. As was the case in fig. 3a uniform spacing of defects is considered (denoted by solid lines) as well as a random spacing of the same number of defects (denoted by dotted lines). Competitive behavior between the defects causes the bulk desorption rate of species 1 and 2 to increase. The production of species 3 at the defects is decreased owing to the reduced trapping of species 1 and 2 by the defects. This results in less of species 3 being supplied to the surface, and therefore a drop in the bulk desorption rate of species 3. This demonstrates that the phenomenon of competitive behavior between defects is not restricted to the simple reactive trapping model considered in fig. 3.

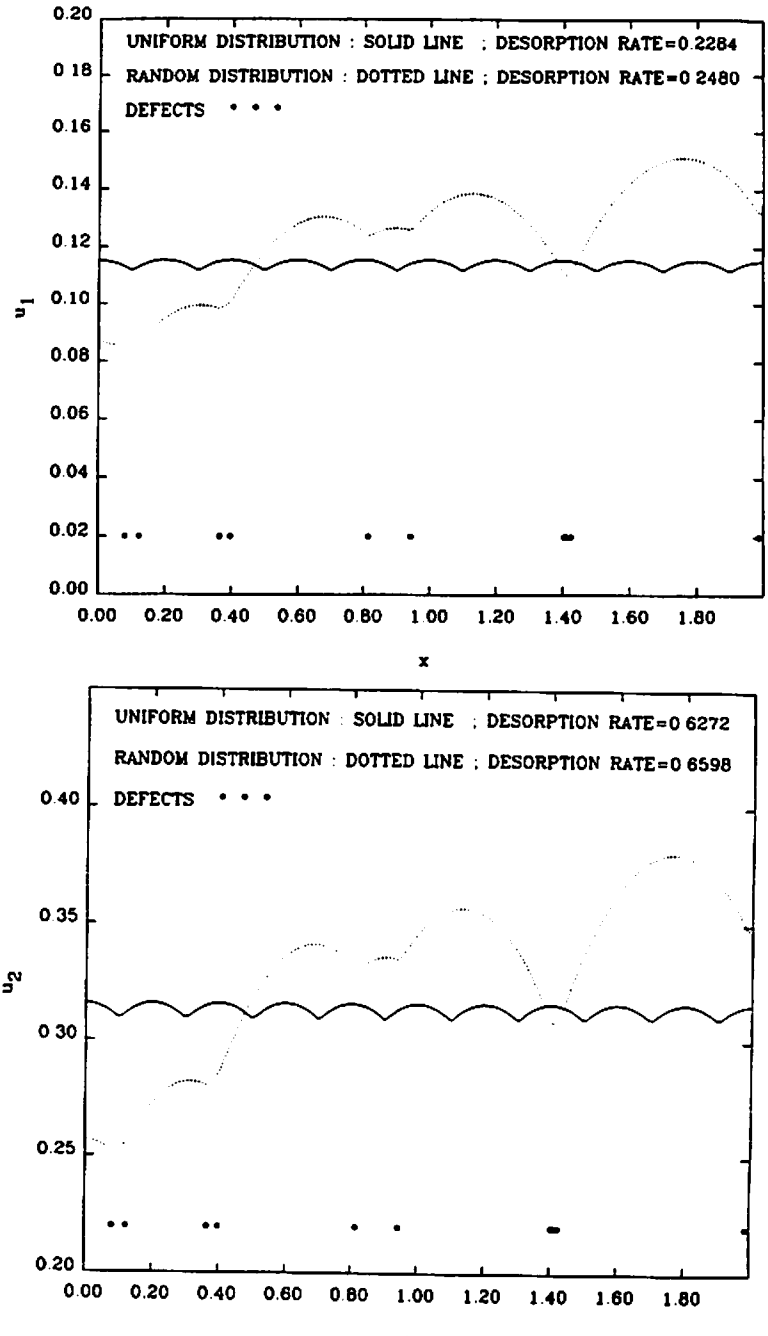

Fig. 4b. The spatial distribution of the concentrations of the three species are plotted at time $t = 4.0$ for both uniformly (solid line) and randomly (dotted line) spaced defects. The locations of the defects are denoted by solid circles toward the bottom of the plots. It is interesting to note the strong relative competitiveness of the two pairs of defects located in the interval [0, 0.4]. This variation of competitiveness with defect spacing causes a redistribution of material between all the defects on the surface.

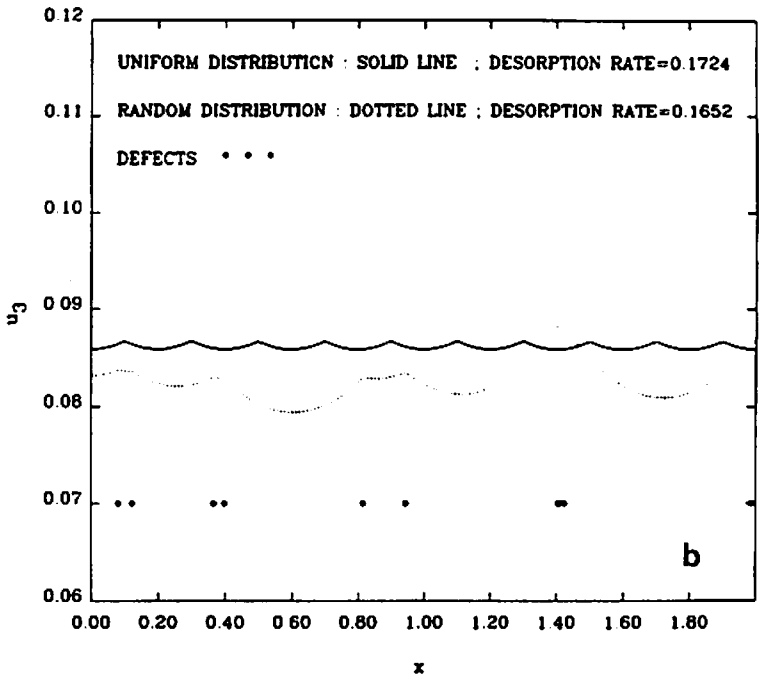

Fig. 4b. Continued.

factors $(s_j - u_j)$ represent saturation at the defects as the concentration of the jth species increases until complete saturation occurs at the concentration s_j. In this section we assume $s_1 = s_2 = 1.0$; $k_1 = 2.0$ and $k_2 = k_3 = 1.0$.

We assume that 10 defects are uniformly spaced over the interval [0, 2.0] so that $L = 0.1$. Then each of the defects is subjected to a finite random perturbation and the adsorption process is repeated. In this case the BE equations are solved using quadratic interpolation and 90 spatial mesh points. The size of the time-step is $\Delta t = 0.01$.

In fig. 4a the time-evolutions of the bulk desorption rates $\mathscr{D}_i$ (defined analogously to (4.10)) for the three species are plotted for uniformly and randomly spaced defects. The competitive behavior between the defects causes the bulk desorption rate of species 1 and 2 to increase when the defects are perturbed from the uniform distribution. Since the concentration of reagents 1 and 2 present at the defects is reduced overall, the production of species 3 at the defects is reduced. This reduced production of species 3 at the defects causes the bulk desorption rate of species 3 to be reduced when the defects are perturbed.

In fig. 4b the spatial distribution of the concentrations of the three species is plotted at time $t = 4.0$ in the case of uniformly spaced defects and randomly

spaced defects. It is interesting to note the relative competitiveness of the pairs of defects centered at $x = 0.1, 0.38, 0.88$ and the three defects located in the interval [1.40, 1.45]. The two pairs located in the interval [0.0, 0.4] are seen to be most competitive while the other groupings of defects are less so. This variation of competitiveness with defect spacing and the existence of a maximum competitiveness at a non-zero defect spacing has been established theoretically [2] and is seen to give rise to interesting redistribution of material in two-dimensional defect structures [13].

This example demonstrates that the phenomenon of competitive behavior between trapping defects is not restricted to simple one-species reactive trapping models such as that considered in section 3.3. It also illustrates the usefulness of the BE algorithm in observing the phenomena in this non-linear environment in which finite perturbations elude analytic treatment. An attempt to predict the outcome of the perturbation process based on physical intuition is difficult because the dominance of competing physical effects has to be determined.

5. Comments and conclusions

In this paper we demonstrated that the proposed numerical algorithm based on the BE technique has the following features:

(i) It provides a convenient representation of the localized non-linear behavior that allows active sites to be modelled by essentially overlaying the effects of the desired active sites without requiring mesh deformation.

(ii) It yields an efficient and convergent algorithm for modelling such localized non-linear behavior which is extremely stable since it exploits the actual Green's function of the linear diffusion process taking place in the bulk medium.

In addition to the representation of localized defects and explicit treatment of the resulting non-linear equations, a further modification to the standard BE algorithm is the incorporation of desorption in the model. Asymptotic methods have been developed to evaluate the solution near boundaries and active sites when desorption is included.

The BE algorithm was applied to a number of interesting physical problems in which non-linear reactions occur at localized defects. In the first problem we considered the Lotka–Volterra system in which the linear source and sink terms and the predator–prey interaction term have been distributed at defect sites in the domain. Material was moved from one site to another by diffusion. This system provided a stringent test of the stability of the BE algorithm as it required that the numerical solution traverse a large portion of the phase plane close to the axis $u_2 = 0$.

In the second problem the BE algorithm was used to consider non-linear effects on marginal oscillations of the Prigogine–Lefever reaction that occurs

at defects. The non-linear terms were seen to introduce small dissipative effects which caused spiraling in toward the marginal stability state. As the trajectory moved closer to the marginal stability state, the dissipative effects of the non-linear terms diminished and a stable cycle behavior was observed.

In the third problem we used the BE algorithm to investigate the effect of defect locations on the balance between desorptive processes on a catalytic surface, assuming dynamic pulsing of the adsorption level. The competitive behavior between defects, which has been established for static adsorption levels, was shown to persist for dynamic loading of the surface. In the fourth problem we demonstrated that the phenomenon of competitive behavior between defects also occurs for a more complex three-species reaction. The latter two examples illustrated the pervasiveness of the competitive behavior exhibited by defect structures on catalytic surfaces.

In sum, the results illustrate the usefulness of the extended BE method for modelling defect structures on catalytic surfaces.

Appendix A: Discretization of BE equations

Let $x_0 < x_1 < \ldots < x_{N-1} < x_N$ be a partition of the interval $[x_0, x_N]$ in which the set of active sites $\{x_{r_l}\}_{l=1}^{L}$ are included as a subset. In accordance with the one time-step recursion algorithm described in sections 3.2 and 3.3, we introduce finite element-like interpolation functions over the rectangular space-time cells $[x_{e-1}, x_e] \times [0, \Delta t]$. Within the eth interval $[x_{e-1}, x_e]$ we introduce the nodal points $\{x_e^a\}_{a=1}^{P}$ and over the time interval we introduce the nodal points $\{t^b\}_{b=1}^{Q}$. Here $P-1$ and $Q-1$ are the degrees of the spatial and time polynomial approximation, respectively. We now define polynomial basis functions X_e^a and T^a:

$$X_e^a: \quad X_e^a(x_K^b) = \delta_{eK}\delta_{ab}, \quad T^a: \quad T^a(t^b) = \delta_{ab}.$$

The resulting interpolants of the functions $u(x, t)$, $\partial u(x_i, t)/\partial \xi = \phi(x_i, t)$ and $f(x, t)$ are obtained:

$$u(x, t_j) = \sum_{e=1}^{N} \sum_{a=1}^{P} X_e^a(x) u(x_e^a, t_j),$$

$$\phi(x_i, t_j + t) = \sum_{b=1}^{Q} T^b(t) \phi(x_i, t_j + t^b), \quad i = 0, N, \tag{A.1}$$

$$f(x, t_j + t) = \sum_{e=1}^{N} \sum_{a=1}^{P} \sum_{b=1}^{Q} X_e^a(x) T^b(t) f(x_e^a, t_j + t^b).$$

Substituting these expressions into (3.3) and assuming homogeneous Dirichlet boundary conditions, we obtain:

$$u(x, t_{j+1}) = \sum_{e=1}^{N}\sum_{a=1}^{P} G^{ea}(x, \Delta t)u^{ea}(t_j) + \sum_{i=0,N}\sum_{b=1}^{Q} g_b^i(x)\phi_b^i(t_j)$$

$$+ \sum_{l=1}^{L}\int_0^{\Delta t} G(x - x_{r_l}, \Delta t - \tau)R_l\left(\sum_{b=1}^{Q} T^b(\tau)u(x_{r_l}, t_j + t^b)\right) d\tau$$

$$+ \sum_{e=1}^{N}\sum_{a=1}^{P}\sum_{b=1}^{Q} G_b^{ea}(x) f_b^{ea}. \qquad \text{(A.2)}$$

Here

$$G^{ea}(x, \Delta t) = \int_{x_{e-1}}^{x_e} G(x - \xi, \Delta t) X_e^a(\xi)\, d\xi,$$

$$g_b^i(x) = \int_0^{\Delta t} G(x - x_i, \Delta t - \tau)T^b(\tau)\, d\tau,$$

$$G_b^{ea}(x) = \int_0^{\Delta t} T^b(\tau)\int_{x_{e-1}}^{x_e} G(x - \xi, \Delta t - \tau) X_e^a(\xi)\, d\xi\, d\tau$$

$$= \int_0^{\Delta t} T^b(\tau)G^{ea}(x, \Delta t - \tau)\, d\tau.$$

It is possible to evaluate the integrals $G^{ea}(x, \Delta t)$ and the self-effects $g_b^i(x_i)$ analytically. In the remaining cases the integrands are smooth and can be evaluated using Gauss integration for points remote from the boundaries. In order to determine the solution for points that are close to boundaries we propose an asymptotic method to evaluate the influence kernels $g_b^i(x)$. This method is outlined in appendix B.

Rather than providing the general expressions of G^{ea} etc. we will provide the analytic expressions for the above kernels in the two special cases $P = Q = 1$ and $P = Q = 2$.

A.1. Interpolation by a constant function in space and time: $P = Q = 1$

In this case

$$x_e^1 = \tfrac{1}{2}(x_{e-1} + x_e), \quad X_e^1 = \{H(x - x_{e-1}) - H(x - x_e)\},$$

where H is the Heavyside function.

$$t^1 = \Delta t, \quad T^1 = \{H(t) - H(t - \Delta t)\},$$

$$(G_{ij})^{e1}(x, \Delta t) = \tfrac{1}{2} \exp(-\Omega_i \Delta t)\left[\operatorname{erf}\left(\frac{x - x_{e-1}}{2\sqrt{D_i \Delta t}}\right) - \operatorname{erf}\left(\frac{x - x_e}{2\sqrt{D_i \Delta t}}\right)\right]\delta_{ij},$$

$$(g_{kl})^i_1(x_i, \Delta t) = \begin{cases} \dfrac{\delta_{kl}}{2\sqrt{D_k \Omega_k}} \operatorname{erf}\left(\sqrt{\Omega_k \Delta t}\right), & \Omega_k \neq 0, \\ \left(\dfrac{\Delta t}{\pi D_k}\right)^{1/2} \delta_{kl}, & \Omega_k = 0. \end{cases} \tag{A.3}$$

Here erf is the error function.

A.2. Interpolation by a linear function in space and time: $P = Q = 2$

In this case

$$x^1_e = x_{e-1}, \quad x^2_e = x_e, \quad X^a_e = \frac{\frac{1}{2}x_e(1 - \theta_a) - \frac{1}{2}x_{e-1}(1 + \theta_a) + \theta_a x}{x_e - x_{e-1}},$$

$$t^1 = 0, \quad t^2 = \Delta t, \quad T^b = \tfrac{1}{2}(1 - \theta_b) + \theta_b t/\Delta t,$$

where

$$\theta_a = \begin{cases} -1, & a = 1, \\ 1, & a = 2, \end{cases}$$

$$(G_{kl})^{ea}(x, \Delta t) = \tfrac{1}{2}\exp(-\Omega_k \Delta t)\left\{\left[\operatorname{erf}\left(\frac{x - x_{e-1}}{2\sqrt{D_k \Delta t}}\right) - \operatorname{erf}\left(\frac{x - x_e}{2\sqrt{D_k \Delta t}}\right)\right] X^a_e(x) + \frac{2\theta_a}{(x_e - x_{e-1})} \frac{D_k \Delta t}{\pi}\left[\exp\left(-\frac{(x - x_{e-1})^2}{4D_k \Delta t}\right) - \exp\left(-\frac{(x - x_e)^2}{4D_k \Delta t}\right)\right]\right\}\delta_{kl}, \tag{A.4}$$

$$(g_{kl})^i_b(x_i, \Delta t) = \begin{cases} \delta_{kl}\left\{\dfrac{1}{2\sqrt{D_k \Omega k}} \operatorname{erf}\left(\sqrt{\Omega_k \Delta t}\right)\left[\tfrac{1}{2}(1 + \theta_b) - \dfrac{\theta_b}{2\Omega_k \Delta t}\right] + \dfrac{\theta_b \exp(-\Omega_k \Delta t)}{2\Omega_k \sqrt{\pi D_k \Delta t}}\right\}, & \Omega_k \neq 0, \\ \delta_{kl} \tfrac{1}{2}(1 + \theta_b/3)\left(\dfrac{\Delta t}{\pi D_k}\right)^{1/2}, & \Omega_k = 0. \end{cases}$$

Appendix B

In appendix A we advocate the use of numerical integration to evaluate the influence matrices

$$g_b^i(x) = \int_0^{\Delta t} G(x - x_i,\ \Delta t - \tau) T^b(\tau)\, d\tau,$$

when $x \neq x_i$. However, when x is close to x_i, standard numerical integration algorithms experience some difficulty owing to the large gradients introduced by the almost singular integrand. If desorption were not present, then this problem would not occur since the required integrals can be evaluated analytically. If desorption is present (i.e., $\Omega_i \neq 0$), then we propose an asymptotic method for calculating these integrals in the limit $x \to x_i$. We provide asymptotic expansions of the integrals that will be required to implement piecewise constant and piecewise linear interpolation schemes.

We assume $|x - x_i| = \epsilon \ll 1$ and define the integrals:

$$g_k(\epsilon) = \int_0^t \frac{\exp\left[-\epsilon^2/4D(t-\tau) - \Omega(t-\tau)\right]}{2\left[\pi D(t-\tau)\right]^{1/2}} \tau^k\, d\tau,$$

then for $\Omega t \ll 1$ we obtain:

$$g_0(\epsilon) = \exp(-\theta^2)\left(\frac{t}{\pi D}\right)^{1/2}\left[1 + \frac{\epsilon^2\Omega}{6D} - \frac{\Omega t}{3}\left(1 + \frac{\epsilon^2\Omega}{20D}\right) + O\left((\Omega t)^2\right)\right]$$

$$- \frac{\epsilon\ \mathrm{erfc}(\theta)}{4D}\left[2 + \frac{\epsilon^2\Omega}{3D} + \frac{\epsilon^4\Omega^2}{60D^2} + O(\epsilon^6)\right],$$

$$g_1(\epsilon) = t g_0(\epsilon) + \frac{\exp(-\theta^2)}{12D^2}\left(\frac{t}{\pi D}\right)^{1/2}\left[-4Dt + 2\epsilon^2\left(1 - \frac{\Omega t}{5}\right) + O(\epsilon^4)\right]$$

$$- \frac{\epsilon^3\ \mathrm{erfc}(\theta)}{12D^2}\left[1 + \frac{\epsilon^2\Omega}{10D} + O(\epsilon^4)\right].$$

Here $\theta = \epsilon/2(Dt)^{1/2}$ and erfc is the complementary error function.

In order to evaluate the near defect effects of the derivative kernels $\partial G/\partial\xi$ in (3.3) we define the integrals

$$g_k'(\epsilon) = \frac{\sigma\epsilon}{4(\pi D^3)^{1/2}} \int_0^t \frac{\exp\left[\epsilon^2/4D(t-\tau) - \Omega(t-\tau)\right]}{(t-\tau)^{3/2}} \tau^k\, d\tau,$$

where $|x - x_i| = \epsilon \ll 1$ and $\sigma = \text{sign}(x - x_i)$. Assuming that $\Omega t \ll 1$ we obtain:

$$g_0'(\epsilon) = \frac{\sigma}{2D}\left\{\text{erfc}(\theta)\left[1 + \frac{\epsilon^2\Omega}{2D} + \frac{\epsilon^4\Omega^2}{24D^2} + O(\epsilon^6)\right]\right.$$
$$\left. - \exp(-\theta^2)\epsilon\Omega\left(\frac{t}{\pi D}\right)^{1/2}\left[1 - \frac{\Omega t}{6} + \frac{\epsilon^2\Omega}{12D}\left(1 - \frac{\Omega t}{15}\right)\right) + O(\epsilon^4)\right]\right\},$$

$$g_1'(\epsilon) = tg_0'(\epsilon) + \frac{\sigma\epsilon}{2D^2}\left\{\frac{\epsilon\ \text{erfc}(\theta)}{4}\left[2 + \frac{\epsilon^2\Omega}{3D} + \frac{\epsilon^4\Omega^2}{60D^2} + O(\epsilon^6)\right]\right.$$
$$\left. + \exp(-\theta^2)\left(\frac{Dt}{\pi}\right)^{1/2}\left[1 + \frac{\epsilon^2\Omega}{6D} - \frac{\Omega t}{12}\left(1 + \frac{\epsilon^2\Omega}{20D}\right) + O\left((\Omega t)^2\right)\right]\right\}.$$

Acknowledgement

The authors acknowledge support for this research from the Office of Naval Research and the Air Force Office of Scientific Research. The first author also gratefully acknowledges the support of the CSIR of South Africa and the Fulbright Foundation.

References

[1] J.A. Serri, J.C. Tully and M.J. Cardillo, J. Chem. Phys. 79 (1985) 1530.
[2] A.P. Peirce and H. Rabitz, Phys. Rev. B, in press.
[3] D.L. Freeman and J.C. Doll, J. Chem. Phys. 78 (1983) 6002; 79 (1983) 2343.
[4] R.I. Cukier, J. Chem. Phys. 79 (1983) 2430.
[5] E.K. Bimpong-Bota, P. Ortoleva and J. Ross, J. Chem. Phys. 60 (1974) 3124.
[6] E.K. Bimpong-Bota, A. Nitzan, P. Ortoleva and J. Ross, J. Chem. Phys. 66 (1977) 3650.
[7] F.F. Grinstein, H. Rabitz and A. Askar, J. Chem. Phys. 82 (1985) 3430.
[8] D. Lee, A. Askar and H. Rabitz, to be published.
[9] P.K. Banerjee and R. Butterfield, Boundary Element Methods in Engineering Science (McGraw-Hill, London, 1981).
[10] C.A. Brebbia and S. Walker, Boundary Element Techniques in Engineering (Newnes-Butterworth, London, 1980).
[11] H.L.G. Pina and J.L.M. Fernandes, Applications in Transient Heat Conduction, in: Vol. 1 of Topics in Boundary Element Research, Ed. C.A. Brebbia (Springer, Berlin, 1984).
[12] A.P. Peirce, A. Askar and H. Rabitz, paper in preparation.
[13] A.P. Peirce and H. Rabitz, Surface Sci. 202 (1988) 32.
[14] W.E. Williams, Partial Differential Equations (Oxford University Press, New York, 1980).
[15] F. John, Partial Differential Equations, 4th ed. (Springer, New York, 1985).
[16] G. Dahlquist and A. Björck, Numerical Methods (Prentice-Hall, Englewood Cliffs, NJ, 1974).